Journal of Applied Mechanics and Technical Physics, Vol. 47, No. 1, pp. 36–46, 2006

CENTRIFUGAL CONVECTION IN RAPID ROTATION OF BODIES MADE OF CELLULAR-POROUS MATERIALS

V. K. Baev, A. V. Fedorov, V. M. Fomin, and T. A. Khmel'

UDC 532.546

Gas flows inside and around rapidly rotating bodies made of cellular-porous materials are studied numerically and experimentally. Within the framework of the previously proposed physicomathematical model, an appropriate numerical algorithm is developed and tested. Internal flows and a conjugate problem with the external flow are considered. The calculated moment and dynamic pressure are in good agreement with experimentally measured characteristics of a rotating porous disk on a solid substrate.

Key words: *cellular-porous materials, rotation, internal and external flows, experiment, numerical simulation.*

Introduction. Highly permeable cellular-porous materials (CPM) found their application as filtering elements and heat- and mass-exchangers in various fields of engineering.

The idea of using these materials and their analogs for manufacturing rotors of multifunctional energy-convecting devices was put forward at the Institute of Theoretical and Applied Mechanics (ITAM) of the Siberian Division of the Russian Academy of Sciences in 2002 and served as a basis for an integration project in basic research [1, 2]. A numerical and theoretical study of external and internal aerodynamics in the case of rotation of permeable bodies was performed in [3].

A physicomathematical model based on principles of mechanics of heterogeneous media was developed in [4]; some new exact and approximate (asymptotic and numerical) solutions were obtained there for one-dimensional and two-dimensional swirl flows inside rotating porous bodies. In the general case, where the drag of a porous structure can be presented as a quadratic or two-term (linear-quadratic) dependence on flow velocity, an analysis of two-dimensional swirl flows can be performed by methods of numerical simulation only. For the full problem of gas motion during rotation of a porous body to be solved, the internal and external flows should be considered together, in a conjugate formulation.

The objectives of the present work are

— numerical and experimental determination of the flow field inside and in the vicinity of a rotating solid CPM body;

— analysis of numerical solutions obtained and their stability;

— determination of the influence of physical parameters (dimensionless length of the cylinder, drag law, and drag coefficients) on the type and character of the flow;

— verification of the proposed mathematical model by comparing numerical results with experimental data.

Physical and Mathematical Formulation of the Problem. A cylindrical CPM body set into rotation around its centerline with a certain angular velocity is considered. Owing to rotation, a forced flow is formed inside the body under the action of centrifugal convection. A mathematical model that describes a steady isothermal flow

Institute of Theoretical and Applied Mechanics, Siberian Division, Russian Academy of Sciences, Novosibirsk 630090; fedorov@itam.nsc.ru; khmel@itam.nsc.ru. Translated from Prikladnaya Mekhanika i Tekhnicheskaya Fizika, Vol. 47, No. 1, pp. 46–57, January–February, 2006. Original article submitted February 9, 2005; revision submitted March 24, 2005.

of an inviscid incompressible gas inside such a body was proposed in [4]. In what follows, it is convenient to use a system of unsteady equations in terms of vorticity and stream function. With allowance for viscous terms, the equations in dimensionless variables in the laboratory (with respect to a motionless observer) cylindrical coordinate system (r, z, θ) fitted to the axis of rotation have the following form:

$$\frac{\partial \chi}{\partial t} - \frac{1}{r}\frac{D(\chi,\psi)}{D(r,z)} = -\frac{1}{r^2}\frac{\partial}{\partial z}w^2 - \frac{1}{r}\Big(\frac{\partial f_z}{\partial r} - \frac{\partial f_r}{\partial z}\Big) + \frac{1}{r^2\,\mathrm{Re}}\Big\{r\frac{\partial}{\partial r}\Big[\frac{1}{r}\frac{\partial (r^2\chi)}{\partial r}\Big] + \frac{\partial^2 (r^2\chi)}{\partial z^2}\Big\},$$

$$\frac{\partial rw}{\partial t} - \frac{1}{r}\frac{D(rw,\psi)}{D(r,z)} = -rf_\theta + \frac{1}{\mathrm{Re}}\Big\{r\frac{\partial}{\partial r}\Big[\frac{1}{r}\frac{\partial (rw)}{\partial r}\Big] + \frac{\partial^2 (rw)}{\partial z^2}\Big\},$$

$$r^2\chi = \frac{\partial^2\psi}{\partial r^2} - \frac{1}{r}\frac{\partial\psi}{\partial r} + \frac{\partial^2\psi}{\partial z^2}, \qquad \frac{D(\chi,\psi)}{D(r,z)} = \frac{\partial\chi}{\partial r}\frac{\partial\psi}{\partial z} - \frac{\partial\psi}{\partial r}\frac{\partial\chi}{\partial z}, \tag{1}$$

$$u = -\frac{1}{r}\frac{\partial\psi}{\partial z}, \qquad v = \frac{1}{r}\frac{\partial\psi}{\partial r}, \qquad \chi = \frac{1}{r}\Big(\frac{\partial v}{\partial r} - \frac{\partial u}{\partial z}\Big).$$

Here u, v, and w are the radial, axial, and azimuthal components of velocity, $\boldsymbol{f}$ is the volume force, χ is the modified vorticity, and ψ is the stream function. The characteristic scales of the problem include the angular velocity of rotation of the body Ω, the characteristic length (outer radius of the cylinder R), the characteristic velocity $R\Omega$, the gas density under standard conditions ρ_0, the time scale $1/\Omega$, and the Reynolds number $\mathrm{Re} = R^2\Omega/\nu$ (ν is the kinematic viscosity). In the general case, the force of interaction between the gas and the porous skeleton is $\boldsymbol{f} = K|\boldsymbol{v} - \boldsymbol{v}_s|(\boldsymbol{v} - \boldsymbol{v}_s) + L(\boldsymbol{v} - \boldsymbol{v}_s)$, where $\boldsymbol{v}_s = r\boldsymbol{i}_\theta$ is the dimensionless velocity of a volume element of the solid skeleton. The dimensional parameters of body drag $k = K/R$ and $\lambda = L\Omega$ depend on material properties, porosity of the structure, and gas viscosity [5]. The external flow is also described by system (1) with $\boldsymbol{f} = 0$.

Numerical Simulation of Internal Flows. A numerical algorithm for solving boundary-value problems for similar equations was developed and successfully used by one of the authors of the present paper to solve problems of external MHD flows of a conducting fluid under the action of electromagnetic fields [6]. The method is based on using Arakawa's conservative scheme [7] for approximating convective terms and solving an elliptic equation for the stream function by an iterative method. The steady-state solution is determined by solving an unsteady problem by a time-dependent method with a nested averaging procedure. The stability and approximating properties of the nested averaging method preventing weak nonlinear Henrici's instability were analyzed in [8]. Two problems were considered to test the numerical method, as applied to the present mathematical model.

Problem 1. *Determination of Stability of the Flow in a Porous Disk with an Internal Cavity within the Numerical Approach Used.* We consider a rotating disk made of a porous material with impermeable end faces $z = 0$ and $z = z_0$ and with an internal cavity of radius r_0, as in [3, 4]. We assume that $L = 0$ in the expression for the drag force, and the values of K are varied. The boundary layer on the end faces is neglected, and the flow at the entrance is assumed to be not swirled. Then the boundary conditions for system (1) have the following form:

$$r = r_0\text{:} \qquad \frac{\partial\psi}{\partial r} = 0, \quad w = 0, \quad \chi = 0,$$

$$r = 1\text{:} \qquad \frac{\partial\psi}{\partial r} = 0, \quad \frac{\partial^2 w}{dr^2} = 0, \quad \frac{\partial\chi}{\partial r} = 0,$$

$$z = 0\text{:} \qquad \psi = 0, \quad \frac{\partial w}{dz} = 0, \quad \frac{\partial\chi}{dz} = 0,$$

$$z = z_0\text{:} \qquad \psi = \Psi, \quad \frac{\partial w}{dz} = 0, \quad \frac{\partial\chi}{dz} = 0.$$

If we neglect the viscous terms and assume that the solution is independent of z, it can be determined from the system of ordinary differential equations (ODE), which follow from system (1) [4]. To solve the problem numerically by a time-dependent method, we use the asymptotic approximation obtained in [4] as part of the initial data:

$$u = \frac{q}{r}, \qquad w = r - \frac{2}{K} + \frac{2}{K^2 r} - \frac{r_0}{r}\Big(r_0 - \frac{2}{K} + \frac{2}{K^2 r_0}\Big)\exp\left[-K(r - r_0)\right].$$

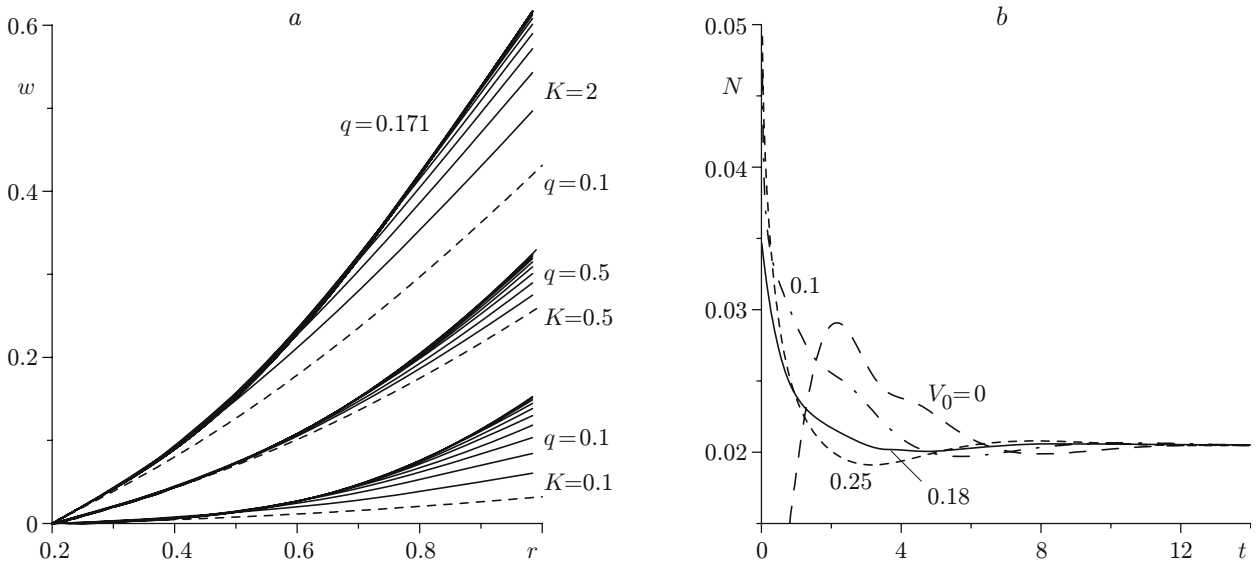

Fig. 1. Convergence of the numerical solution in Problem 1 (transition from the asymptotic to the limiting solution) (a) and Problem 2 (behavior of the total pressure integral for different initial data) (b).

The exact value of the flow rate q is obtained by an iterative method from the relation

$$-w_1^2 = 2\int\limits_{r_0}^{1}\Big(\frac{w^2}{r} - f_r\Big)\,dr, \tag{2}$$

which follows from the Bernoulli integral at the entrance and at the exit [4]. A similar iterative procedure allows us to determine the value of ψ in the course of solving the time-dependent problem in a two-dimensional domain. Using the presentation $u_{n+1} = u_n(1+\sigma)$ (we assume that σ is small) and linearization of condition (2) with respect to a small increment σu_n, we can find

$$\sigma = \left[\int\limits_0^{z_0} w(1,z)^2\,dz + 2\int\limits_{r_0}^{1}\int\limits_0^{z_0}\Big[\frac{w^2}{r} - Ku_n\sqrt{u_n^2+(w-r)^2}\,\Big]\,dr\,dz\right]\Bigg/\left[2\int\limits_{r_0}^{1}\int\limits_0^{z_0}\frac{K[2u_n^2+(w-r)^2]}{\sqrt{u_n^2+(w-r)^2}}\,dr\,dz\right]; \tag{3}$$

correspondingly, we have $\psi_{n+1} = (1+\sigma)\psi_n$. The procedure is repeated at each time step and allows us to satisfy condition (2) as the steady-state solution is approached.

Numerical solutions obtained by using the above-described algorithm are plotted in Fig. 1a for $r_0 = 0.2$ and different values of K in the form of azimuthal velocity profiles with a certain time step. The dashed curves show the initial profiles (asymptotic solution); the limiting curves merge in the graph with the solutions of the ODE system [4]. Both for given values of q ($K = 0.1$ and $q = 0.1$; $K = 0.5$ and $q = 0.5$) and with allowance for relation (2) ($K = 2$), the numerical solution monotonically approaches the solution of the ODE system. With the use of procedure (3), the flow rate q in a steady flow is 0.171, which coincides with data for the same value $K = 2$ obtained in [4].

Retaining of the steady solution in the unsteady problem and convergence to the steady solution in the iterative problem with close initial data indicate that the solution is stable to infinitesimal perturbations and low-amplitude finite disturbances. Calculations with arbitrary initial data revealed the following feature. If the initial value of the flow rate is higher than the true value, the iterative procedure (3) is diverging. For initial data with low flow rates (including those with the zero initial value of q), the iterations converge, and the solution obtained by a time-dependent method also corresponds to the solution of the ODE system.

Problem 2. *Internal Two-Dimensional Flow in a Rotating Cylinder.* A two-dimensional axisymmetric swirl flow inside a cylinder rotating in free space is numerically simulated. The domain $0 \leqslant r \leqslant 1$, $0 \leqslant z \leqslant z_0$ is considered; the boundary conditions have the form

$$r = 0: \qquad \psi = 0, \quad w = 0, \quad \chi = 0,$$

$$r = 1: \qquad \frac{\partial^2 \psi}{\partial r^2} = 0, \quad \frac{\partial^2 w}{dr^2} = 0, \quad \frac{\partial^2 \chi}{dr^2} = 0,$$

$$z = 0: \qquad \frac{\partial \psi}{\partial z} = -r^2 U_0, \quad w = 0, \quad \chi = 0,$$

$$z = z_0: \qquad \psi = 0, \quad \frac{\partial w}{dz} = 0, \quad \frac{\partial \chi}{dz} = 0.$$

For $K = 0$, the solution can also be obtained from an appropriate ODE system [4]. The initial conditions were varied from the distribution corresponding to the solution of the ODE system for a linear drag law to zero values of all functions. The accuracy was controlled by estimating the numerical functional

$$N = \Delta_r \Delta_z \sum_i \sum_j [p_{ij} + 0.5(u_{ij}^2 + v_{ij}^2 + w_{ij}^2)] r_i$$

and determining the residue $\Delta N = N - N_*$, where N_* is calculated by solving the ODE system [4]. The solution was found to converge with grid refinement; in particular, for $K = 0$, $L = 1$, $z_0 = 0.5$, and $U_0 = 0$, the values of the residue $\Delta N = N - N_*$ on a sequence of grids 21×21, 41×41, and 81×81 were 0.00032, 0.000084, and 0.000022, respectively. The steady solution is also independent of the initial approximation, which can be seen in Fig. 1b, which shows the time evolution of the functional N in calculating the time-dependent problem with $K = 1$, $L = 0$, $z_0 = 0.5$, and $U_0 = 0$. The initial data here were the solutions of the ODE system [4] obtained for $K = 0$ and different values of L [the corresponding values of $V_0 = v(0, r)$ are plotted in Fig. 1b].

Two-dimensional flow patterns are shown in Fig. 2a in the form of streamlines and isolines of azimuthal velocity, pressure, and total pressure $P = p + 0.5(u^2 + v^2 + w^2)$. The pressure in the steady flow was determined by integrating equations of motion in the conventional form under the condition that the Bernoulli integral of the incoming flow $p(0, 0) + v(0, 0)^2/2 = 0$ was satisfied. With allowance for $\chi(r, 0) = 0$, this yields

$$p(r, z) = -\frac{v(r, z)^2}{2} - \frac{u(r, 0)^2}{2} - \int_0^z f_z(r, z)\, dz - \int_0^r f_r(r, 0)\, dr.$$

The pressure in the entire domain has negative values, reaching a minimum at the output boundary $r = 1$. The total pressure is negative in the region adjacent to the axis of symmetry and the plane of symmetry, positive in the region $r > 0.5$, $z > 0.1$, and substantially higher than zero at the exit.

Figure 2b and c illustrates the effect of deviation of the incoming flow on the solution ($U_0 \neq 0$) and shows the streamlines and the pressure distributions for positive and negative values of U_0. Comparing Figs. 2a, 2b, and 2c, we can note that the value and sign of U_0 affect the distribution of input and output sections. The maximum values of ψ, which determine the flow rate, reach 0.083 (for $U_0 = 0$), 0.088 (for $U_0 = 0.04$), and 0.079 (for $U_0 = -0.1$). Thus, the flow rate is lower for negative values of U_0, and the inflow partly occurs through the side surface of the cylinder. The distributions of azimuthal velocity for $U_0 = 0.04$ and $U_0 = -0.1$ almost coincide with those plotted in Fig. 2a for $U_0 = 0$. Concerning the total pressure, changes in U_0 affect the shape and position of the zero isoline and the magnitude of pressure at the exit ($r = 1$). This indicates that obtaining reliable information on the internal distribution of parameters and integral characteristics, such as dynamic pressure and flow rate, which strongly depend on the flow pattern, requires coupled consideration of the internal and external flows.

Solution of the Conjugate Problem for the Internal and External Flows. The conjugate problem is solved by domain-through computations with the use of the above-described numerical algorithm both for the internal and for the external flow. Formulation of the boundary conditions depends on whether the volume where the body rotates is open or closed. The computations were performed both in a closed volume with no-slip conditions on the surfaces $z = 0$, $z = z_1$, and $r = r_1$, and in an open volume with "soft" input and output conditions in the form

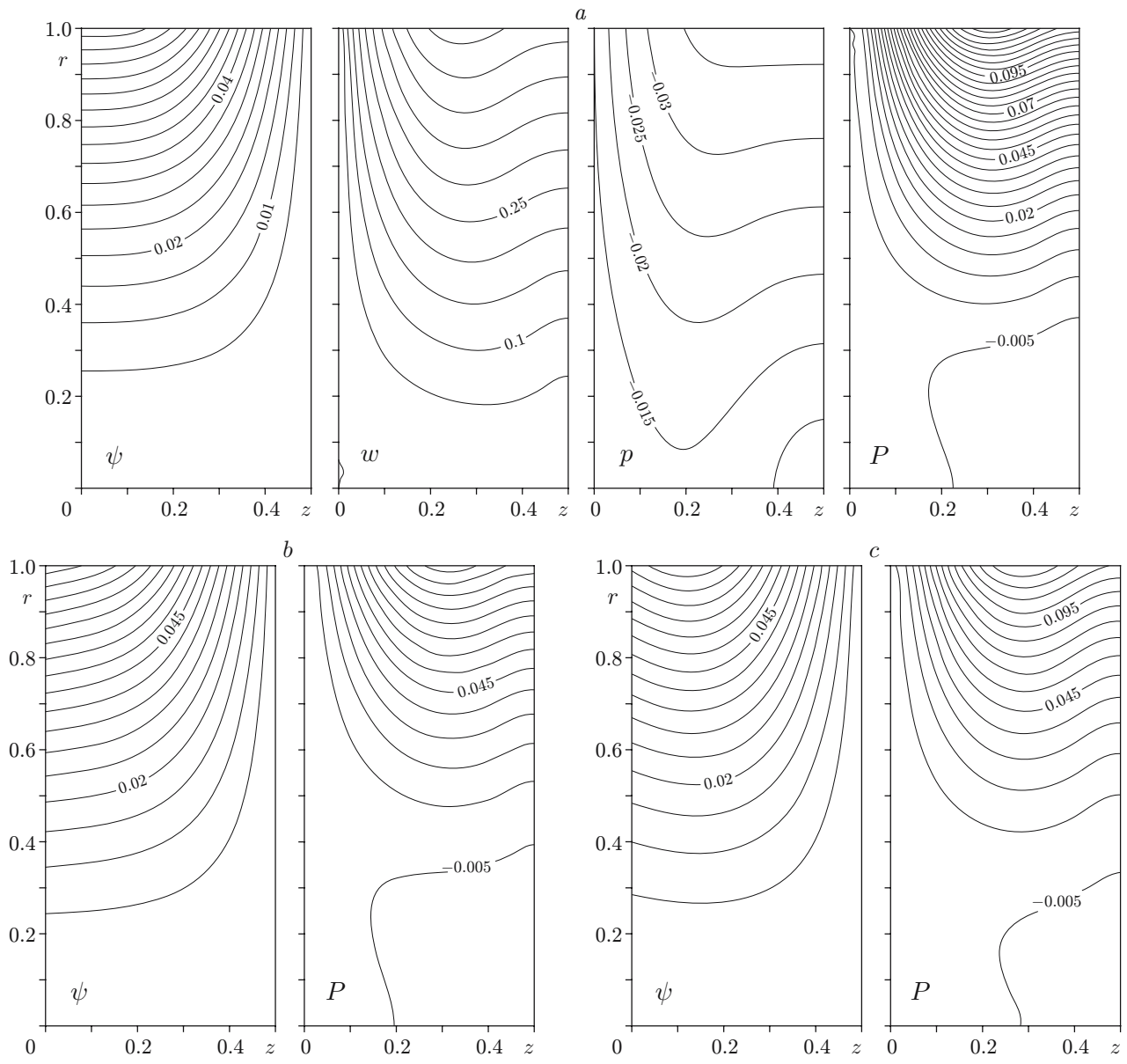

Fig. 2. Two-dimensional patterns of the internal flow for $U_0 = 0$ (a), 0.04 (b), and -0.1 (c).

$$\frac{\partial\psi(r,z)}{\partial z}\Big|_{z=0} = 0, \qquad \chi(r,0) = 0, \qquad w(r,0) = 0,$$

$$\frac{\partial^2\psi(r,z)}{\partial r^2}\Big|_{r=r_1} = 0, \quad \frac{\partial^2\chi(r,z)}{\partial r^2}\Big|_{r=r_1} = 0, \quad \frac{\partial^2 w(r,z)}{\partial r^2}\Big|_{r=r_1} = 0 \quad \text{at} \quad u(r_1,z) > 0, \tag{4}$$

$$\chi = 0, \quad w = 0 \qquad \text{at} \quad u(r_1,z) \leqslant 0.$$

The conditions at the axis of symmetry and in the plane of symmetry $z = z_1$ were the same as those in Problem 2. The flow patterns inside the rotating disk with $z_0 = 0.5$, $K = 1$, $L = 0$, $\Delta z = 0.0125$, and $\Delta r = 0.025$ are plotted in Fig. 3a ($z_1 = 5$, $r_1 = 10$; closed volume) and in Fig. 3b ($z_1 = 1$, $r_1 = 3$; open volume). We had $\psi_{\max} = 0.0673$ (Fig. 3a) or 0.0671 (Fig. 3b) on the porous body surface. As the solution coincided and close values of the flow rate were obtained, we confined ourselves in what follows to computations in an open volume with "soft" boundary

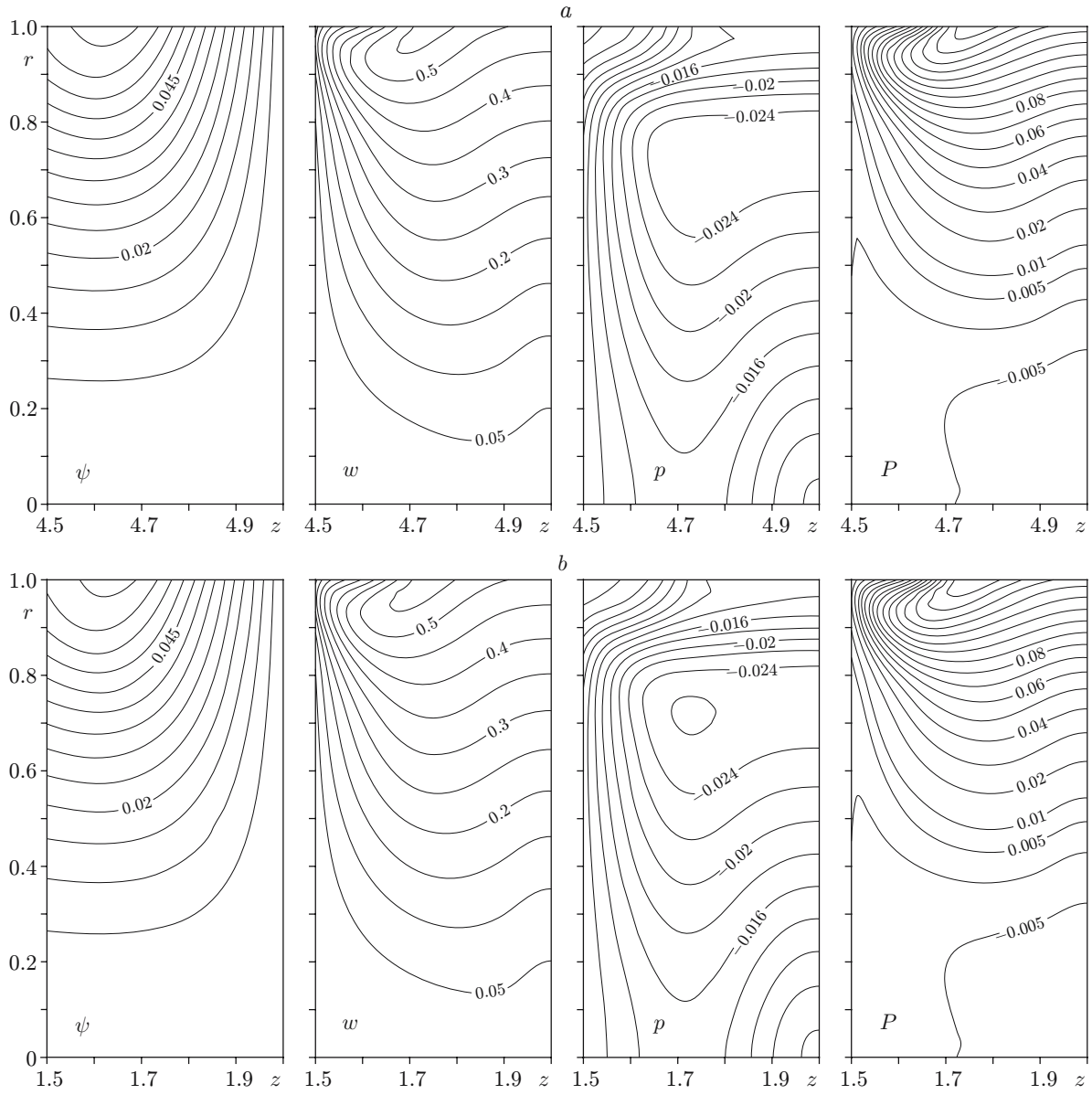

Fig. 3. Internal flows in solving the conjugate problem in a large closed volume (a) and in a small open volume (b).

conditions (4). The computations were performed for different values of K (from 1 to 50) and for three values of z_0: 0.1, 0.2, and 0.5.

The character of the flow with $K = 1$ and $z_0 = 0.5$ (Fig. 3) corresponds to the solution of Problem 2 (for the internal flow) under the condition $U_0 < 0$ on the incoming flow (see Fig. 2c). The inflow here proceeds both through the end face and partly through the side surface of the cylinder. The isolines of the azimuthal component of velocity differ from those in Fig. 2a, though the maximum values of w are also reached on the surface. With decreasing z_0, the inflow region passes to the end face, and the flow pattern for $z_0 = 0.1$ is similar to that in Fig. 2b for $U_0 > 0$.

The flow rates ($\psi_{\max}$ on the porous body surface) for different drag parameters K and dimensionless length of the cylinder z_0 are given in the first three columns of Table 1. The flow rate as a function of z_0 is monotonically increasing and nonlinear with a tendency to saturation ($\psi_{\max} = 0.0607$ for $K = 50$ and $z_0 = 1$). We can assume

TABLE 1

Flow Rate and Moment of Disk Rotation as Functions of the Dimensionless Thickness and Drag Parameter

K	$\psi_{\max}$			M		
	$z_0 = 0.1$	$z_0 = 0.2$	$z_0 = 0.5$	$z_0 = 0.1$	$z_0 = 0.2$	$z_0 = 0.5$
1	0.0155	0.0304	0.0671	0.0525	0.104	0.235
5	0.0201	0.0392	0.0827	0.103	0.202	0.426
10	0.0195	0.0383	0.0779	0.113	0.222	0.430
25	0.0166	0.0321	0.0643	0.102	0.195	0.389
50	0.0133	0.0255	0.0508	0.0868	0.163	0.318

that there exists a limiting value of the flow rate for $z_0 \to \infty$. The dependence of the flow rate on the drag parameter K is nonmonotonic, and a value of K at which the maximum flow rate is reached can be determined for each particular z_0.

The moment of the force necessary to sustain rotation of the porous disk with a prescribed constant angular velocity is balanced by the integral moment of the circumferential drag force and is determined as $M = \iint\limits_V 2\pi r^2 f_\theta \, dr \, dz$. The last three columns of Table 1 give the values of the moment M for different values of z_0 and K. It is seen that the maximums in the dependence $M(K)$ do not coincide with the maximums in $\psi_{\max}(K)$. Thus, we can find a value of K at which the maximum ratio of the flow rate to the moment is reached (as for a disk with closed end faces and an internal cavity [4]). The dependence of the moment on z_0 is also monotonically increasing, whereas the ratio $\psi_{\max}/M$ increases for $K < 5$ and decreases for $K > 5$ with rather insignificant variations. This behavior does not allow finding the optimal geometric relations in terms of $\psi_{\max}/M$ for a fixed value of K. Both M and $\psi_{\max}/M$ tend to reach a "plateau" with increasing z_0 ($\psi_{\max}/M = 0.0160$ for $K = 50$ and $z_0 = 0.5$; $\psi_{\max}/M = 0.0161$ for $z_0 = 1$). The revealed properties can be useful for design of devices based on the use of rotating bodies made of cellular-porous materials.

Calculation of the Experimental Model. A disk made of cellular-porous copper (150 mm in diameter and 20 mm thick) rotating in open space was experimentally studied at ITAM. One side of the disk was covered by a continuous thin-walled copper disk alloyed to the cellular-porous structure during manufacturing.

The photograph and schematic of the setup are shown in Fig. 4. To measure the drag-force moment, the disk was mounted on the electric motor axis resting on two ball-bearing supports (Fig. 4b), whereas the stator (motor casing) was restrained from motion by an arm resting on a force-measurement strain-gauge device calibrated by static loading of the arm. The dynamic pressure was measured by a total pressure probe moved by a traversing gear with respect to the disk.

The flow around the disk was preliminary visualized by the smoking wire method. It was shown that inflow conditions are substantially affected by objects located at distances smaller than the disk radius. Therefore, the free space on the inflow side had nothing except for the pressure probe.

Figure 5 shows the measured moment for different values of the angular velocity and tangential velocity in the middle part of the side surface of the disk.

The disk motion was calculated within the framework of the model described above. Note that there are no reliable data on drag parameters of the material used. The cellular-porous structure is nonuniform, but the mean parameters of the pore size, character of wire roughness, and calculated value of material porosity are close to those of one of the samples considered in [5] (sample No. 38). Correspondingly, the drag law is assumed to be the two-term formula [5] $\Delta p/h = \alpha_0 u + \beta_0 u^2$, and the experimentally measured coefficients for sample No. 38 [5] $\alpha_0 = 2 \cdot 10^7$ m^{-2} and $\beta_0 = 690$ m^{-1} allow us to determine the values of $L = \alpha_0 \nu/\Omega = 1.5\omega$, where ν is the kinematic viscosity of the gas, $\omega = \Omega_0/\Omega$, $\Omega_0 = 2000$ rpm, and $K = \beta_0 R = 51.5$. Other parameters in the computations were taken in accordance with the experimental data: $R = 0.075$ m, $z_0 = z/R = 0.25$, and $\rho_0 = 1.3$ kg/m^3. The computations were performed in an open volume $0 \leqslant z \leqslant 0.5$, $0 \leqslant r \leqslant 1.5$ subject to the boundary conditions (4); the porous body size was $0.25 \leqslant z \leqslant 0.5$, $0 \leqslant r \leqslant 1$. The conditions $w = r$ and $\partial u/\partial z = 0$ were imposed on the solid impermeable substrate.

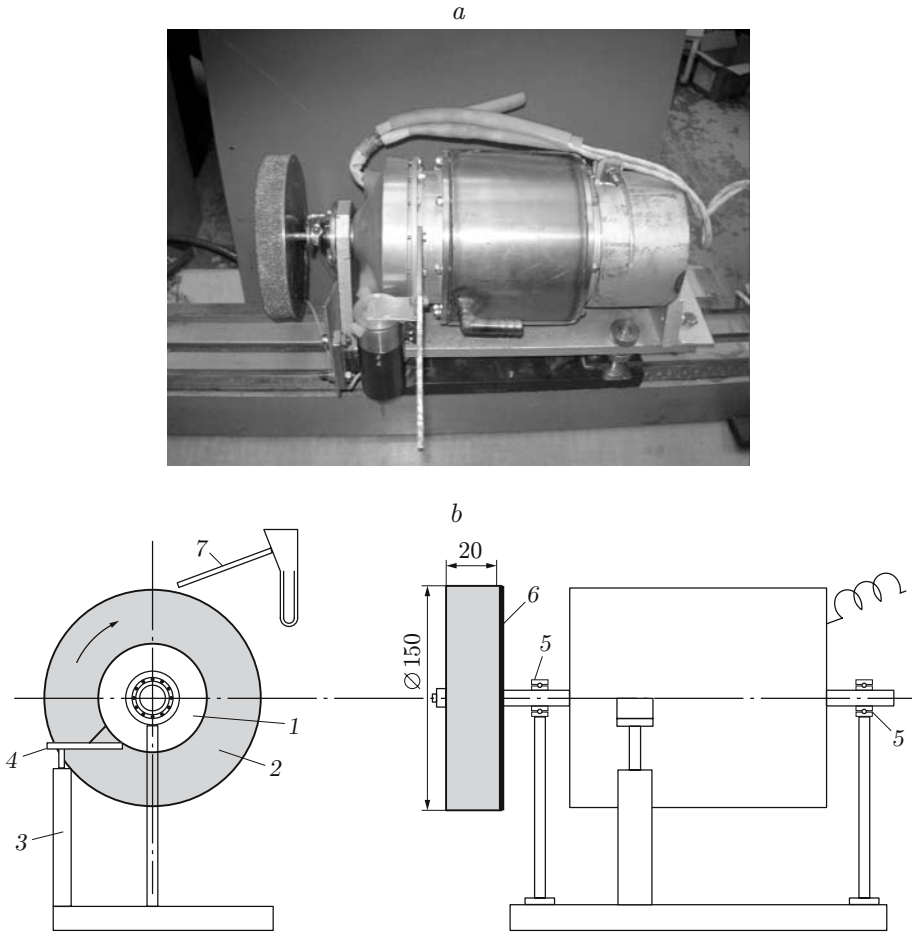

Fig. 4. Experimental setup for studying rotating CPM bodies: (a) photograph; (b) schematic: electric motor (1), cellular-porous disk (2), force-measurement element (3), arm (4), ball-bearing supports (5), impermeable wall (6), and total pressure probe (7).

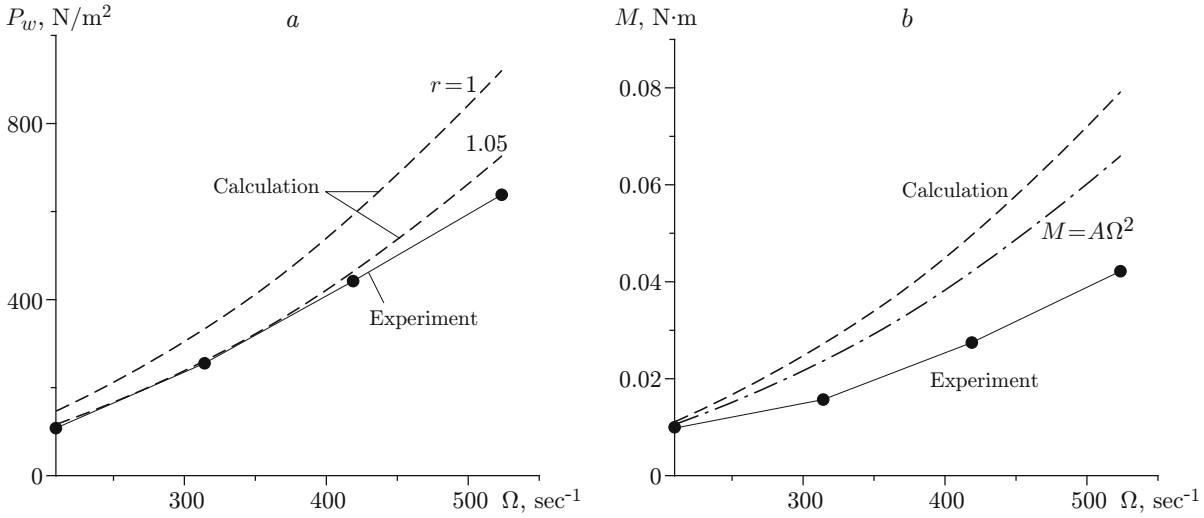

Fig. 5. Dynamic pressure in the azimuthal direction (a) and moment of the rotation force (b) versus the angular velocity of disk rotation.

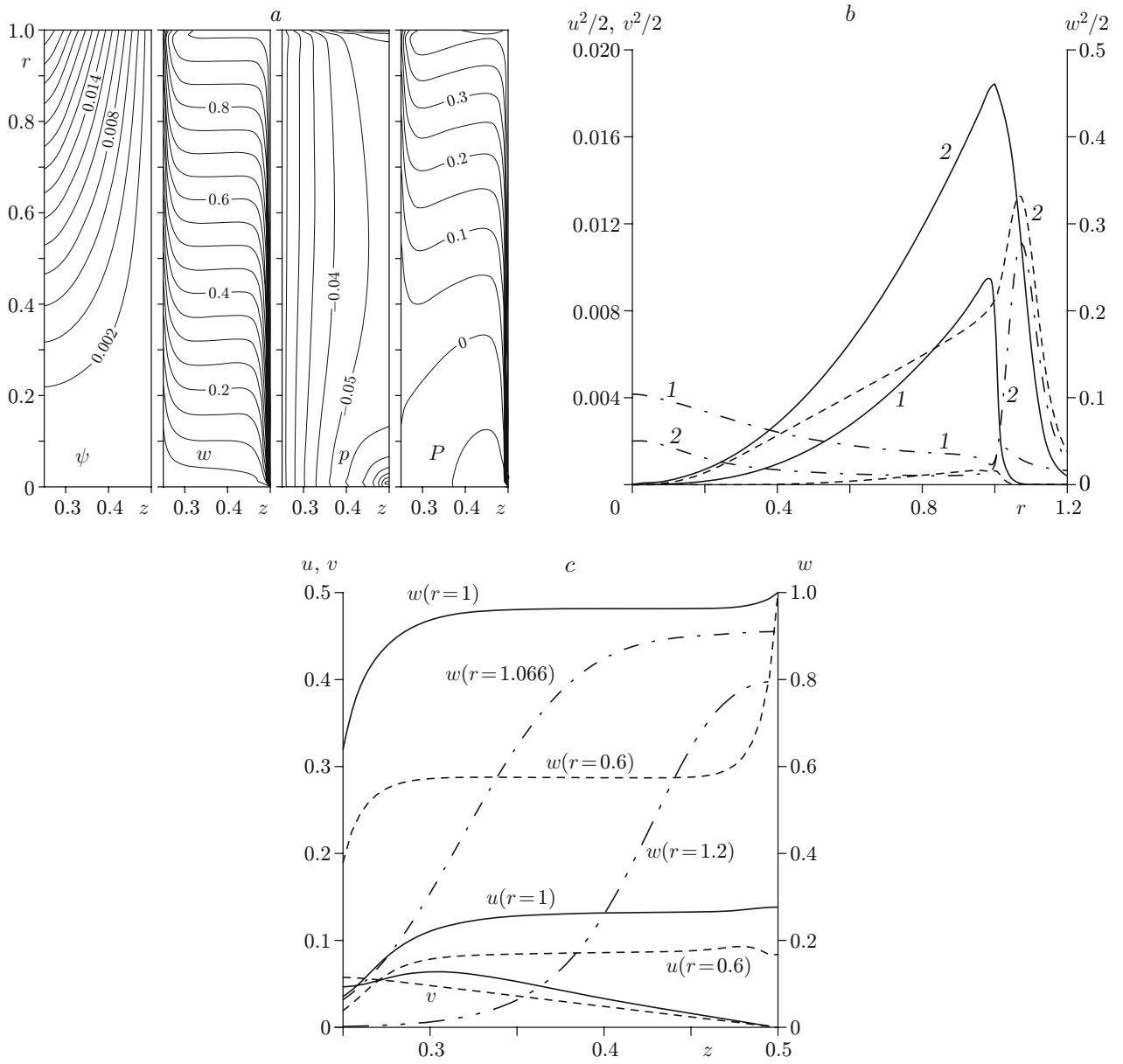

Fig. 6. Flow inside the experimentally tested disk: (a) two-dimensional patterns; (b) profiles of parameters in the cross sections $z = 0.25$ (1) and 0.375 (2); (c) velocity components as functions of z for different values of r.

The computed results are plotted in Fig. 6. Figure 6a shows the two-dimensional patterns of the flow in the form of isolines of the main parameters. The profiles of dynamic pressure in different directions and velocity components in different cross sections inside and in the vicinity of the rotating body for $\omega = 1$ ($\Omega = 2000$ rpm) are shown in Figs. 6b and 6c, respectively. It is seen from Fig. 6b that the main contribution to the total dynamic pressure is main by the azimuthal component w, whereas two remaining components (plotted on the left ordinate axis) are comparatively small. It is also seen in Figs. 6b and 6c that the maximum values of azimuthal velocity and dynamic pressure in the middle cross section ($z = 0.25$) are reached on the side surface of the cylinder, and their values rapidly decrease with distance from the surface ($r > 1$). The range of variation of w along the axis increases drastically thereby (see Fig. 6c). The computed azimuthal component of dynamic pressure $P_w = 0.5\rho_0 R^2\Omega^2 w^2$ is compared with its values measured near the side surface in the middle part of the disk in Fig. 5a. The computed

data (dashed curves) are plotted for the values $r = 1$ and $r = 1.05$ (which refers to the distance from the surface equal to 3.75 mm) and correspond to a quadratic dependence on angular velocity. The experimental curve is close to the predicted curve for $r = 1.05$ and $\Omega < 400$ sec^{-1} (up to 4000 rpm) but somewhat deviates as the angular velocity increases.

The computed values of the moment

$$M = \rho_0 R^5 \Omega^2 \int_{0.25}^{0.5} \int_{0}^{1} 2\pi r^2 f_\theta \, dr \, dz$$

are in good agreement with experimental results for $\Omega = 2000$ rpm (about 200 sec^{-1}; see Fig. 5b), but some difference is observed with increasing Ω. An analysis of the drag law also yield an exponential dependence of the force and moment on Ω with an exponent of 2 for high values of Ω. The corresponding curve $M = A\Omega^2$ passing through the first experimental point is shown by the dot-and-dashed curve in Fig. 5b. The difference at high values of Ω can be caused by the experimental error or by ignoring some of the factors in computations (e.g., the volume of the nut that partly overlapped the inflow cross section was neglected). Within the assumptions made, the agreement between experimental and numerical data is fairly reasonable.

Conclusions. Flows inside bodies made of cellular-porous materials rotating with high angular velocities are examined theoretically and experimentally.

A numerical technology for studying conjugate internal and external incompressible gas flows inside and in the vicinity of rapidly rotating bodies made of cellular-porous materials is developed within the theoretical model based on principles of mechanics of continuous media. The numerical algorithm is based on application of Arakawa's explicit finite-difference scheme, an iterative method for the stream function, and a procedure of nested averaging for obtaining stable solutions by a time-dependent method. The numerical method is tested on two problems, which demonstrate the convergence and stability of the numerical solution. The computation results obtained in a comparatively small open volume with appropriate "soft" input and output conditions are shown to be reliable.

The influence of the governing parameters of the problem on the flow patterns and types is analyzed. The effect of the incoming flow direction and dimensionless length of the cylinder on the character of the internal flow is revealed. The possibility of obtaining flows with an inflow section on the side surface of the rotating cylindrical body is demonstrated. The effect of the drag parameter and geometric relations on the flow rate of the fluid through the porous body and on the moment of the rotation force is found.

Experimentally measured moment and dynamic pressure for a rotating disk made of a cellular-porous material on a solid substrate are presented. Numerical simulations of the flow pattern inside and outside a similar sample with the use of the model and algorithm proposed ensure satisfactory agreement in terms of local and integral characteristics as functions of angular velocity.

The mathematical model and the numerical method can be developed to study nonisothermal flows. As the equation for temperature in the Boussinesq equation is similar to the vorticity equation, it can also be solved by the numerical algorithm developed.

The authors are grateful to A. D. Frolov and A. Ya. Korotkikh for obtaining the experimental data and to Z. R. Ismagilov for availability of the disk made of a cellular-porous material.

This work was supported by the Russian Foundation for Basic Research (Grant No. 03-01-00453) and by the Siberian Division of the Russian Academy of Sciences (Integration Project No. 83).

REFERENCES

1. V. K. Baev and V. M. Fomin, "Main ideas of interdisciplinary projects of new types of energy-transducing facilities," in: *Proc. of the Int. Conf. on Methods of Aerodynamic Research* (Novosibirsk, Russia, June 28–July 3, 2004), Part I, Publ. House "Nonparallel," Novosibirsk (2004), pp. 26–29.
2. V. K. Baev and V. M. Fomin, "Multifunctional machines with disk rotors," in: *Energy Saving and Provision of Ecological Safety on Industrial Enterprises*, Proc. of the Conf. (St. Petersburg, Russia, May 26–28, 2004), St. Petersburg Electrotechnical Company, St. Petersburg (2004), pp. 7–9.

3. V. K. Baev and S. S. Minaev, "Characteristics of the flow around and inside of the rotating porous disk," in: *Book of Abstracts of Advanced Fluid Information and Transdisciplinary Fluid Integration*, Tohoku University, Sendai, Japan (2004), pp. 238–241.
4. A. V. Fedorov, V. M. Fomin, and T. A. Khmel', "Mathematical modeling of flows inside rotating bodies made of cellular-porous materials," *J. Appl. Mech. Tech. Phys.*, **46**, No. 6, 835–841 (2005).
5. A. M. Beklemyshev, "Specific features of the drag law in high-porous cellular materials," Republican Engineering Center of Powder Metallurgy and Institute of Problems of Powder Technology and Coatings and Pilot Production, Perm' (1996). Deposited at VINITI, 07.09.96, No. 2265-B96.
6. T. A. Pupykina, "Numerical calculation of inviscid MHD flow around complex-shaped bodies," in: *Numerical Methods of Mechanics of Continuous Media* (collected scientific papers) [in Russian], Vol. 16, No. 4, Inst. Theor. Appl. Mech., Sib. Div., Acad of Sci. of the USSR, Novosibirsk (1985), pp. 95–110.
7. P. J. Roache, *Computational Fluid Mechanics*, Hermosa, Albuquerque (1976).
8. M. I. Zhilyaev and T. A. Pupykina, "Modification of a central difference scheme for calculating two-dimensional inviscid flows in force fields," in: *Numerical Methods of Mechanics of Continuous Media* (collected scientific papers) [in Russian], Vol. 14, No. 3, Inst. Theor. Appl. Mech., Sib. Div., Acad of Sci. of the USSR (1983), pp. 65–75.